# On the spurious solutions in the high-order finite difference methods for eigenvalue problems

## S. Zhao [*]

*Department of Mathematics, University of Alabama, Tuscaloosa, AL 35487, USA*

## Abstract

In this paper, the origins of spurious solutions occurring in the high-order finite difference methods are studied. Based on a uniform mesh, spurious modes are found in the high-order one-sided finite difference discretizations of many eigenvalue problems. Spurious modes are classified as spectral pollution and non-spectral pollution. The latter can be partially avoided by mesh refinement, while the former persists when the mesh is refined. Through numerical studies of some prototype eigenvalue problems, such as those of the Helmholtz and beam equations, we show that perfect central differentiation schemes do not produce any spurious modes. Nevertheless, high-order central difference schemes encounter difficulties in implementing complex boundary conditions. We further show that the central difference schemes will produce spurious modes as well, if asymmetric approximation is involved in boundary treatments. In general, central difference schemes are less likely to produce spurious modes than one-sided difference schemes.
© 2007 Elsevier B.V. All rights reserved.

*Keywords:* Spurious modes; Spectral pollution; High-order finite differences; Central difference schemes; Boundary condition implementation; Matched interface and boundary method

## 1. Introduction

Spurious solution or spurious mode is a widely used term in physics [5,9], mathematics [2–4,8,13,14], and engineering [6,7,12,15], to refer to a non-physical solution that bears no resemblance to the actual one. However, there is no rigorous or precise definition of spurious solution in general. In fact, two spurious solutions raised from different fields may have little in common except that they are both non-physical. Sometimes, a spurious solution may just mean an unwelcome or unexpected artifact [15]. To avoid an unwelcome spurious solution, one has to find out its true origin, which in general could be due to either physical and mathematical modelings, or numerical methods.

A typical example of spurious solutions induced by physical modeling is the one resulting from the multiband

$\mathbf{k} \cdot \mathbf{p}$ model theory of envelope structures [5,9]. Spurious solutions induced by mathematical modeling are usually due to the missing of certain analytical constraints in mathematical formulations. In computational electromagnetics, it has been shown [12] that the divergence equation is an essential part of Maxwell's equations. If the divergence free constraint is neglected, a zero-frequency mode becomes a solution of Maxwell's equations [4]. Consequently, spurious modes with non-zero frequencies arise in numerical solutions. Similarly, in the vibration analysis of fluid–solid systems, it has been found [2] that if the zero-frequency circulation mode is not prevented in displacement formulation, a non-physical sub-space related to the zero-frequency eigenvalue is appended to the spectrum of discrete matrices.

The most interesting spurious solutions are those that are directly related to numerical methods, i.e., spurious solutions induced by algorithm. Spurious solutions induced by algorithm may also arise from the loss of constraint during the process of the numerical discretization. For

[*] Tel.: +1 205 348 5155; fax: +1 205 348 7067.
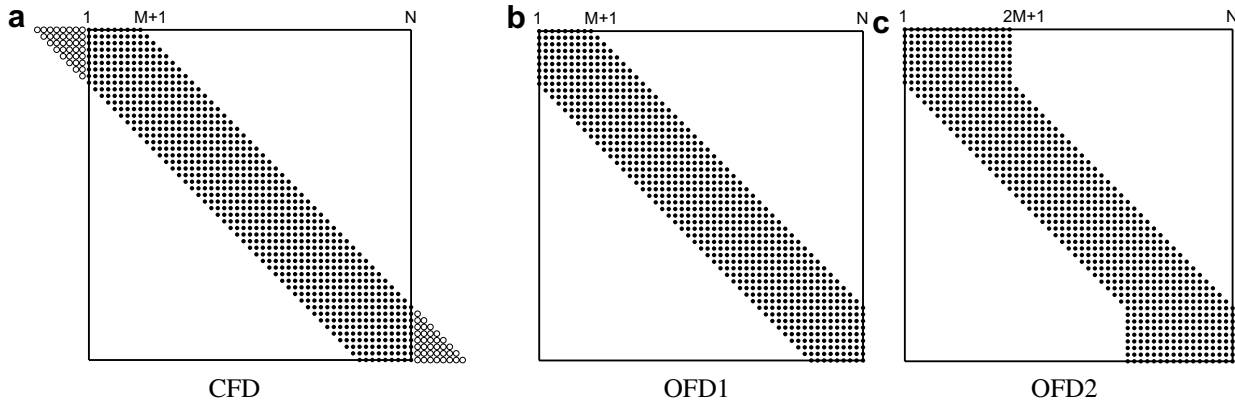*E-mail address:* szhao@bama.ua.edu

Fig. 1. Illustration of the matrix structures of high-order finite difference methods. (a) Central finite difference (CFD); (b) one-sided finite difference type 1 (OFD1); (c) one-sided finite difference type 2 (OFD2).

example, spurious modes induced by algorithm occur if the imaginary part is simply dropped to save half of the computational effort in a real-part boundary element method [6,7]. In this work, we will consider two types of spurious solutions induced by algorithm. The first type, as discussed above, is due to the loss of certain constraints in a particular discretization scheme. Such a loss leads to a larger eigensolution space. As a result, the discrete matrix possesses eigenvalues which are unrelated to any spectrum of the original operator. Such an eigensolution may sometimes be referred to as spectral pollution in the mathematical literature [8,14]. Denote $\text{Spec}(A)$ and $\text{Spec}(A_N)$, respectively, to be the spectrum of original operator $A$ and of the corresponding discrete matrix $A_N$, with $N$ being the meshsize. A point $\lambda$ is said to be spectral pollution of $A$, if there exist $\lambda_N \in \text{Spec}(A_N)$ such that $\lambda_N \to \lambda$ as $N \to \infty$ but $\lambda$ does not belong to $\text{Spec}(A)$. It is noted that spurious solutions induced by mathematical modeling are spectral pollution too, since they are also due to the loss of constraints. The other type of spurious solutions induced by algorithm is a non-spectral pollution one. Numerically, this type of spurious modes will not converge. Instead, the discrete matrix has different spurious eigenvalues when using different grid, because these spurious solutions are not essential to the discrete operator $A_N$. In the present study, the non-spectral pollution spurious solutions are found to be linked to asymmetric approximation to the self-adjoint operator, even though the necessary constraints are not missing.

It is noted that the aforementioned examples of spurious solutions are often only restricted to a particular field, and are seldom studied in the contexts of different disciplines. Clearly, there is a lack of systematic and multidisciplinary studies in the literature, although such studies could have tremendous impact on various fields in physical, mathematical, and engineering sciences.

The objective of this work is to study the origin of spurious solutions induced by numerical discretizations. In particular, we investigate spurious solutions generated by using both central finite difference (CFD) and one-sided

finite difference (OFD) schemes. Some prototype problems such as eigenvalue problems of the Helmholtz and Beam equations are considered in this paper, while the findings of this work should be true for general eigenvalue problems. It is well known that by employing a large stencil, high-order CFD schemes encounter difficulties in dealing with complex boundary conditions, because a translation invariant CFD differentiation kernel will refer to grid points outside the domain, see Fig. 1a. One approach to bypass this difficulty is to use one-sided differentiations near boundaries such that only grid points inside the domain will be deployed. Two typical OFD methods will be investigated in this paper, see Fig. 1b and c, although it is possible to consider other types of OFD matrix structures. However, such possibilities will not affect the essential conclusion of the present study. Another approach is to maintain the CFD in the whole computational domain by using fictitious domain outside the boundary. This approach has not been possible until a recent progress in high-order methods, the development of matched interface and boundary (MIB) method [25]. The MIB method is reformulated from a recently developed interface scheme, the hierarchical derivative matching [22,23], originally proposed for simulating electromagnetic wave scattering and propagation in inhomogeneous media. The MIB method has been generalized for the elliptic equations with curved interfaces [26] and various boundary conditions [24].

The rest of this paper is organized as follows. In Section 2, several relevant boundary closure methods are reviewed. In Section 3, we show how to completely or partially avoid spurious modes. A conclusion is given in Section 4.

## 2. Mathematical apparatus

To facilitate our discussion of spurious solutions, we first consider boundary closure techniques in high-order central finite difference (CFD) and one-sided finite difference (OFD) schemes. Throughout the paper, we will consider only a uniform grid with a total of $N$ regular grid points along each dimension, e.g., along the $x$-direction,

we have the grid $x_1 = a < x_2 < \cdots < x_N = b$, where $[a,b]$ is the domain interval. In the present study, one approach is referred to as a stable scheme if it is free of spurious solutions. When one scheme is less likely to produce spurious modes than another, the former will be said to be more stable than the latter. The instability here is not the time-integration instability of unsteady problems.

### 2.1. Boundary treatments in one-sided finite different schemes

In the high-order OFD methods, in order to avoid the boundary closure difficulty of applying a CFD kernel in a translation invariant manner, progressively more asymmetric finite difference approximations to the governing partial differential equation (PDE) are employed near the boundaries [11,17,24]. Boundary conditions will be implemented by means of OFD approximations without using nodes outside the computational domain.

#### 2.1.1. One-sided finite different approximations
The OFD approximation is defined pointwisely

$$u^{(n)}(x_i) = \sum_{j=S_1}^{S_2} c_{i,j}^{(n)}(x_i)u(x_j), \tag{1}$$

where $u^{(n)}(x_i)$ is the $n$th order derivative of $u(x_i)$, and $S_1$ and $S_2$ are the summation limits. The OFD Lagrange kernels $c_{i,j}^{(n)}(x_i)$ can be given as

$$c_{i,j}(x) = \prod_{k=S_1, k \neq j}^{S_2} \frac{x - x_k}{x_j - x_k}, \tag{2}$$

$$c_{i,j}^{(n)}(x_i) = \left. \frac{d^n c_{i,j}(x)}{dx^n} \right|_{x=x_i}. \tag{3}$$

The above differentiation of the Lagrange interpolation kernel can be carried out analytically. In this paper, a fast algorithm which is able to determine weights in high-order finite difference formulas on arbitrarily spaced grids [10] will be employed to calculate the OFD coefficients. We note that if the summation (1) is global, i.e., $S_1 = 1$ and $S_2 = N$, this actually gives a differential quadrature approximation [16].

Different choice of the summation limits $S_1$ and $S_2$ gives rise to different OFD matrix structures. Two typical OFD methods shown in Fig. 1b and c will be considered in this paper, although others can be similarly studied. For both OFD methods, symmetric finite difference kernel with fixed bandwidth $2M + 1$ is used for interior nodes, i.e., $S_1 = i - M$ and $S_2 = i + M$, as long as it is not beyond the domain. Here, $M$ clearly characterizes the order of accuracy of the finite difference approximation. Near boundaries, asymmetric finite difference kernels are employed. These two methods use different limits $S_1$ and $S_2$ for summation (1) at $x_i$

- OFD1

$$S_1 = \max(i - M, 1), \quad S_2 = \min(i + M, N), \tag{4}$$

- OFD2

$$S_1 = \max(\min(i - M, N - 2M), 1),$$
$$S_2 = \min(\max(1 + 2M, i + M), N), \tag{5}$$

where $1 \leqslant i \leqslant N$ and $2M + 1 \leqslant N$.

As shown in Fig. 1, the matrix structure of OFD1 is the same as that of CFD. There seems no reason to consider a OFD method with even shorter stencil at the boundaries. The OFD2 method essentially aims to maintain the same order of accuracy throughout the domain by using one-sided finite difference kernels with fixed bandwidth $2M + 1$ near the boundaries, see Fig. 1c. Even longer OFD kernels will not improve the order of convergence. We thus only focus on these two OFD methods in the present study. We will show that the OFD2 method is more accurate than the OFD1 method, while the latter is more stable than the former.

To facilitate the stability discussion in the next section, we denote the degree of asymmetry of the OFD1 and OFD2 as $\{0{:}2M\}$ and $\{0{:}M\}$, respectively. Here $\{M_1{:}M_2\}$ denotes that the most asymmetric approximation in a high-order finite difference discretization has $M_1$ and $M_2$ nodes, respectively, from the left and right side of the point of differentiation. If the most asymmetric stencil is for the right boundary, the values of $M_1$ and $M_2$ will be interchanged. Thus, one always has that $M_2 \geqslant M_1$. The degree of asymmetry of a central finite difference method is $\{M{:}M\}$.

#### 2.1.2. Boundary closure methods for the OFD
To impose boundary conditions in both OFD1 and OFD2, one should first discretize boundary conditions by means of OFD approximations. This usually gives rise to two algebraic equations at $x_1$ and $x_N$, i.e., two endpoints. There are different boundary closure methods to incorporate these two boundary algebraic equations into the entire PDE discretization. We will consider the following two schemes:

- *Boundary closure scheme 1*
  In scheme 1, algebraic equations attained from discretized boundary conditions at $x_1$ and $x_N$ are simply coupled with the algebraic equations attained from the discretized PDE at $x_2, \ldots, x_{N-1}$. This straightforward boundary method is often assumed in the text books of numerical analysis for the standard finite difference method. However, it may yield spurious solution in higher dimensions as we will demonstrate in the next section.
- *Boundary closure scheme 2*
  In scheme 2, one first solves two boundary algebraic equations to determine $u_1$ and $u_N$. In particular, $u_1$ and $u_N$ will be represented as linear combinations of $u_2, \ldots, u_{N-1}$. Then when $u_1$ and $u_N$ is referred in discretizing the PDE on inner nodes $x_2, \ldots, x_{N-1}$, the

representations of $u_1$ and $u_N$ in terms of $u_2, \ldots, u_{N-1}$ will be supplied, so that the final finite difference matrix will not involve $u_1$ and $u_N$. In other words, the resulting discrete matrix thus has a dimension of $(N-2) \times (N-2)$. This type boundary treatment is commonly used in the differential quadrature method [16].

Here we consider an example to illustrate the scheme 2. More examples of both boundary closure methods are available in Ref. [24]. We consider the eigenvalue analysis of double free-edged beams [25]. The dimensionless governing equation is

$$\frac{\mathrm{d}^4 W}{\mathrm{d}x^4} = k^2 W, \tag{6}$$

where $W$ is the displacement and $k$ is the frequency parameter. On both ends of the domain, the free edge support is assumed

$$\frac{\mathrm{d}^2 W}{\mathrm{d}x^2} = 0, \quad \frac{\mathrm{d}^3 W}{\mathrm{d}x^3} = 0. \tag{7}$$

It is noted that since there are two boundary conditions to be imposed on each boundary, the boundary closure scheme 1 is not applicable. One can only solve this eigenvalue problem via the scheme 2. In the following, we will discuss the boundary implementation in the context of the differential quadrature method [16]. The differential quadrature approximation can be obtained by taking $S_1 = 1$ and $S_2 = N$ in (1)

$$u^{(n)}(x_i) = \sum_{j=1}^{N} C_{i,j}^{(n)} u(x_j), \tag{8}$$

here for simplicity we denote $C_{i,j}^{(n)} = c_{i,j}^{(n)}(x_i)$. Consequently, the governing Eq. (6) can be discretized as

$$\sum_{j=1}^{N} C_{i,j}^{(4)} W_j = k^2 W_i, \quad i = 1, 2, \ldots, N \tag{9}$$

and the free edge boundary conditions can be discretized as

$$\sum_{j=1}^{N} C_{1,j}^{(2)} W_j = 0, \tag{10}$$

$$\sum_{j=1}^{N} C_{1,j}^{(3)} W_j = 0, \tag{11}$$

$$\sum_{j=1}^{N} C_{N,j}^{(2)} W_j = 0, \tag{12}$$

$$\sum_{j=1}^{N} C_{N,j}^{(3)} W_j = 0. \tag{13}$$

Eqs. (10)–(13) can be expressed in the matrix form such that

$$B_B W^{(S)} + B_D W^{(I)} = 0, \tag{14}$$

where $W^{(S)} = [W_1, W_2, W_{N-1}, W_N]^{\mathrm{T}}$, $W^{(I)} = [W_3, W_4, \ldots, W_{N-3}, W_{N-2}]^{\mathrm{T}}$. $B_B$ and $B_D$ are $4 \times 4$ and $4 \times (N-4)$ matrix

respectively. Similarly, Eq. (9) can be expressed in the matrix form

$$D_B W^{(S)} + D_D W^{(I)} = k^2 W^{(I)}, \tag{15}$$

where $D_B$ and $D_D$ are $(N-4) \times 4$ and $(N-4) \times (N-4)$ matrix respectively. Eq. (14) can be coupled with Eq. (15) to give

$$D_D W^{(I)} - D_B B_B^{-1} B_D W^{(I)} = k^2 W^{(I)}, \tag{16}$$

$$(D_D - D_B B_B^{-1} B_D) W^{(I)} = k^2 W^{(I)}. \tag{17}$$

Finally, Eq. (17) can be expressed as a problem of eigenvalues and eigenvectors

$$[A][W^{(I)}] = k^2 [W^{(I)}]. \tag{18}$$

This procedure essentially solves boundary values $W^{(S)} = [W_1, W_2, W_{N-1}, W_N]^{\mathrm{T}}$ from Eqs. (10)–(13) by means of interior values $W^{(I)} = [W_3, W_4, \ldots, W_{N-3}, W_{N-2}]^{\mathrm{T}}$. Then the approximation of the governing equation at inner nodes $(x_3, x_4, \ldots, x_{N-3}, x_{N-2})$ is modified after these boundary value representations are taken into account, to form a $(N-4) \times (N-4)$ dimension matrix $[A]$. This is exactly the boundary closure scheme 2 discussed above. The same boundary treatment can be applied to both OFD1 method and OFD2 method. In such a case, boundary treatments for the left and right ends can be conducted separately, because Eqs. (10) and (11) are decoupled with Eqs. (12) and (13).

Although we focus on only two boundary closure schemes, we note that there are other boundary closure methods for the OFD formulation. For example, by admitting the same number of fictitious points as that of the boundary conditions at an edge, a local adaptive differential quadrature method has been recently proposed [18]. The boundary method in that work is essentially the closure scheme 2 discussed above, except that the boundary points to be dropped are actually fictitious points. Thus, the final discretization is formed on the entire domain $(x_1, x_2, \ldots, x_N)$ [18].

### 2.2. Boundary closure methods for central finite difference

In the standard $(2M)$th order central finite difference (CFD) approximation, the derivative of a function is approximated via a weighted linear sum involving $2M + 1$ nodes,

$$u^{(n)}(x) = \sum_{j=-M}^{M} c_j^{(n)}(x) u(x_j), \tag{19}$$

where the translation invariant finite difference kernel $c_j^{(n)}(x)$ is the $n$th order derivative of the Lagrange interpolation kernel

$$c_j(x) = \prod_{k=-M, k \neq j}^{M} \frac{x - x_k}{x_j - x_k}. \tag{20}$$

Similarly, the fast algorithm [10] will be used to generate CFD coefficients.

To maintain the use of one CFD kernel in a translation invariant manner, one must accurately estimate function values on the fictitious domains outside the domain $[a, b]$, i.e., $(x_{1-M}, \ldots, x_0)$ and $(x_{N+1}, \ldots, x_{N+M})$ for a $(2M)$th order CFD scheme, based on the given boundary conditions, see Fig. 1a. Once these fictitious values are determined via certain fictitious domain boundary treatments, a $2M + 1$ point CFD approximation can be used for all regular nodes $(x_1, x_2, \ldots, x_N)$. The essential challenge in high-order CFD methods is that the number of available boundary conditions is far less than those required for the determining of $M$ fictitious points outside each boundary [24].

### 2.2.1. Treatment without one-sided approximations

The fictitious values can be attained in an exact sense for some simple boundary conditions, such as the periodic condition [19], the asymptotic Dirichlet condition [21], the perfect electric and magnetic wall conditions in electromagnetic [1], the simply supported, clamped and transversely supported edges in vibration analysis [20], etc. In these cases, one can simply assume that there is a one-to-one correspondence between the inner nodes and the outer fictitious nodes on the boundary [20]. For example, we assume that for the left boundary

$$u(x_{1-j}) - u(x_1) = a_j[u(x_{1+j}) - u(x_1)] \qquad (21)$$

where $a_j$, for $j = 1, 2, \ldots, M$, is the unknown representation coefficient to be determined from the boundary conditions. In the context of the discrete singular convolution algorithm [19], this fictitious domain boundary technique is usually referred to as a boundary extension. For example, at a clamped edge, the boundary conditions

$$u(x_1) = 0, \quad u^{(1)}(x_1) = 0 \qquad (22)$$

will be realized via the symmetric extension $a_j = 1$, $j = 1, 2, \ldots, M$. At a simply supported edge, boundary conditions

$$u(x_1) = 0, \quad u^{(2)}(x_1) = 0 \qquad (23)$$

can be imposed via the anti-symmetric extension $a_j = -1$, $j = 1, 2, \ldots, M$. However, the one-to-one assumption (21) might not be rigorously valid for more complex boundary conditions [24,25].

### 2.2.2. Treatment involving one-sided approximations – the matched interface and boundary (MIB) method

The difficulty of implementing general boundary conditions in the discrete singular convolution algorithm motivates the development of the matched interface and boundary (MIB) method, for accurately treating various boundary conditions. To illustrate the idea, we consider the Neumann boundary condition at the left boundary

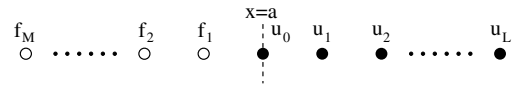$$u_x = \phi \quad \text{at } x = a. \qquad (24)$$



Fig. 2. Illustration of fictitious points near the left boundary.

The MIB method introduces a fictitious domain outside the boundary (see Fig. 2), and repeatedly matches the boundary condition across the boundary. Referring to the Fig. 2, we denote the fictitious values on the $M$ fictitious points outside the domain as $f_i$ for $i = 1, 2, \ldots, M$, while the function values of the $L + 1$ grid points inside the domain which are involved in the MIB modeling are denoted as $u_j$ for $j = 0, 1, 2, \ldots, L$. Note that index $j$ begins at $0$. We seek for a high-order approach to represent $f_i$ in terms of $u_j$ by means of discretizing boundary condition (24).

At the first step, since only one boundary condition is available, one can only determine one fictitious point, i.e., $f_1$. In order to achieve high-order accuracy for the boundary implementation, we employ one-sided finite difference approximations, which involve $L + 1$ grid points on the inner side of the boundary; see Fig. 3. Thus, boundary condition (24) is approximated by using an $L + 2$ point finite difference approximation

$$C_{2,1}^{(1)} f_1 + \sum_{i=2}^{L+2} C_{2,i}^{(1)} u_{i-2} = \phi, \qquad (25)$$

where $C_{2,i}^{(1)}$ for $i = 1, \ldots, L + 2$ are the one-sided finite difference weights for the first order derivative at point 2. We note that the degree of asymmetry of this approximation is $\{1:L\}$. The only unknown $f_1$ in Eq. (25) can be solved in terms of $u_i$ for $i = 0, \ldots, L$ and $\phi$. Here, we note the flexibility of choosing the total number of terms used by varying $L$ in the finite difference approximation. While the length of $L$ determines the level of accuracy, it can be either larger or smaller than $M$. To ensure the stability, in practice, $L > 12$ is hardly used.

To gain a sufficient number of function values at fictitious points, we use an iterative procedure as introduced in electromagnetic interface problems. By treating the previous calculated fictitious point as knowns, we seek for determining one more fictitious point at one time as shown in Fig. 3. Numerically, this is accomplished by discretizing the same boundary condition again, but with one new fictitious point

$$C_{3,1}^{(1)} f_2 + C_{3,2}^{(1)} f_1 + \sum_{i=3}^{L+3} C_{3,i}^{(1)} u_{i-3} = \phi, \qquad (26)$$

where $C_{3,i}^{(1)}$ for $i = 1, \ldots, L + 3$ are the one-sided finite difference weights for the first order derivative with its differentiation at point 3. The grid partition considered in (26) still has $L + 1$ inner nodes, but two fictitious points outside the boundary. Thus, this partition is independent of the previous one. Moreover, this approximation is less asymmetric than that of the first step, with the degree $\{2:L\}$. Since $f_1$ has already been determined from Eq. (25), $f_2$ can be solved from
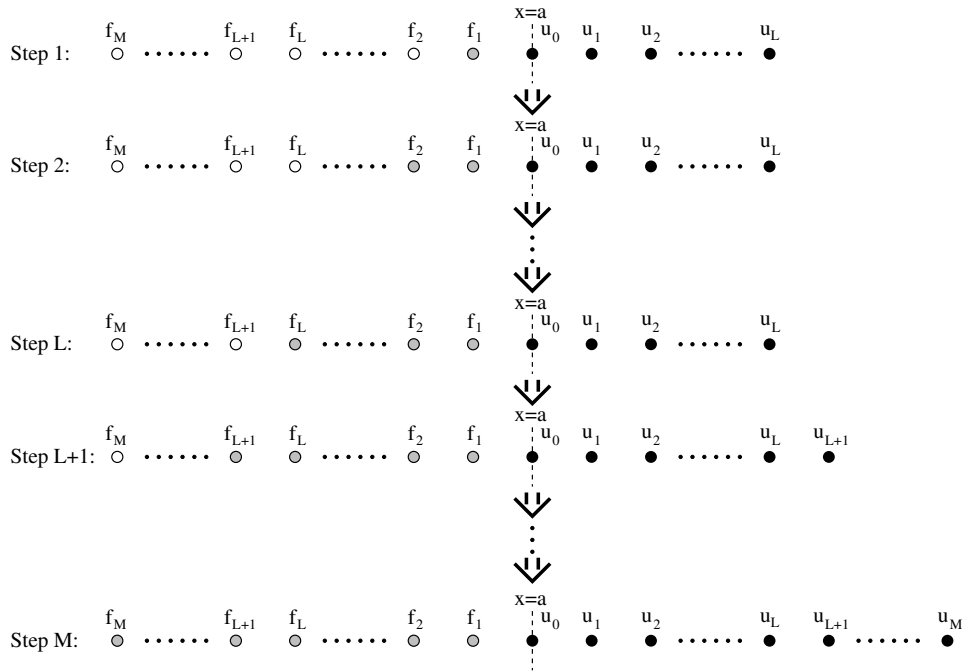
Fig. 3. Illustration of the iterative procedure.

(26). Through such an iterative procedure, the required $M$ fictitious points can be efficiently determined if $M \leqslant L$. Then the degree of asymmetry of the last step will be $\{M{:}L\}$.

To ensure the stability at the first step of the MIB method, $L$ cannot be very large. Nevertheless, in practice, $M$ could be quite large. Thus, one need to consider the case with $M > L$. Then, more iterative steps are required. Through the above procedure, at step $L$, one can determine $f_i$ for $i = 1, 2, \ldots, L$. Now, at step $L + 1$, a central finite difference weights will be employed so that boundary condition (24) is discretized as

$$\sum_{i=1}^{L+1} C_{L+2,i}^{(1)} f_{L+2-i} + \sum_{i=L+2}^{2L+3} C_{L+2,i}^{(1)} u_{i-L-2} = \phi. \quad (27)$$

In other words, from step $L + 1$ onward, one will add both one more fictitious points and one more grid point at each iterative step in the MIB iteration, as shown in Fig. 3. This is because central finite difference approximations are not only more accurate but also more stable than one-sided finite difference approximations. In Eq. (27), one still has only one unknown, i.e., $f_{L+1}$, which can be easily solved. One can repeat this procedure as many times as necessary, until the desired $M$ fictitious points are all determined, see Fig. 3. The degree of asymmetry will be $\{L + 1{:}L + 1\}, \{L + 2{:}L + 2\}, \ldots, \{M{:}M\}$ in successive steps.

In order to apply the MIB method to a boundary value or eigenvalue problem in which $u_j$ is not readily available, a fundamental representation is essential for an implicit formulation

$$f_i = \mathbf{R}^i \cdot \mathbf{U} \quad \text{for } i = 1, 2, \ldots, M, \quad (28)$$

where vector $\mathbf{U} = (u_0, \ldots, u_L, \phi)$ and the elements of vector $\mathbf{R}^i$ are the representation coefficients of $f_i$ with respect to $\mathbf{U}$.

With this representation, instead of solving $f_i$, one needs to determine $\mathbf{R}^i$. Representation coefficients $\mathbf{R}^i$ will be determined from essentially the same procedure presented above for $f_i$. The only difference is that now one boundary condition is discretized and coupled into $L + 2$ algebraic equations, since a fictitious value $f_i$ is represented via $L + 2$ coefficients which are $L + 2$ elements of $\mathbf{R}^i$.

Since the procedure of implementing boundary condition is systematic, the MIB method can be of arbitrarily high order in principle. The MIB method provides a fictitious domain support so that a high-order CFD kernel can be applied in a translation invariant manner throughout the domain. Although one-sided approximations are used in determining fictitious values, CFD schemes are strictly used for the discretization of the differential equation. Consequently, the present CFD-MIB method hardly produces spurious solutions. This feature will be carefully investigated in the next section.

## 3. Results and discussions

In this section, we examine the occurrence of spurious modes in various finite difference schemes. Spectral pollution and non-spectral pollution spurious solutions will be studied, respectively, in the following two subsections. We will show that there are two sources of non-spectral pollution spurious solutions. The first source is due to the asymmetric boundary treatment. The other is due to the asymmetric discretization of the differential equation.

A uniform grid will be employed in all cases, with $N$ being the meshsize along each Cartesian grid direction. The bandwidth of the central finite difference (CFD) is $2M + 1$, which is the same as that of the one-sided finite

difference (OFD) for interior nodes. Both boundary closure schemes discussed in Section 2.1.2 will be considered for the OFD1 and OFD2 (see Fig. 1). The following five benchmark problems whose analytical solutions are available are employed to study the origins of spurious modes.

- Simply supported beam [20],

$$\frac{d^4 W}{dx^4} = k^2 W, \quad x \in [0, \pi],$$
$$W(0) = W^{(2)}(0) = 0,$$
$$W(\pi) = W^{(2)}(\pi) = 0. \tag{29}$$

- Beam with free edges [25]

$$\frac{d^4 W}{dx^4} = k^2 W, \quad x \in [0, \pi],$$
$$W^{(2)}(0) = W^{(3)}(0) = 0,$$
$$W^{(2)}(\pi) = W^{(3)}(\pi) = 0. \tag{30}$$

- 1D Helmholtz equation with Dirichlet boundary conditions

$$u_{xx} + k^2 u = 0, \quad x \in [0, \pi],$$
$$u(0) = 0, \quad u(\pi) = 0. \tag{31}$$

- 1D Helmholtz equation with Neumann boundary conditions

$$u_{xx} + k^2 u = 0, \quad x \in [0, \pi],$$
$$u_x(0) = 0, \quad u_x(\pi) = 0. \tag{32}$$

- 2D Helmholtz equation with Neumann boundary conditions

$$\Delta u + k^2 u = 0, \quad \text{in } \Omega = [0, \pi] \times [0, \pi],$$
$$\frac{\partial u}{\partial n} = 0, \quad \text{on } \Gamma = \partial \Omega. \tag{33}$$

The physical eigenvalues of these benchmark problems are all real. In the present study, a numerical eigenvalue whose imaginary part absolute value is greater than a threshold value $\epsilon = 10^{-4}$, will be counted as a spurious mode. In all Tables of this paper, for the purpose of identifying spurious modes easily, an imaginary part that originally should be given as 0.0000 to match the real part, will be simply reported as 0.0. Moreover, all numerical eigenvalues will be sorted according to their magnitudes, so that we can investigate the first occurrence of spurious mode in the spectrum of the discrete matrix. This gives an idea how much the discrete spectrum is polluted. The RG routine from the EISPACK is employed to computer eigenvalues in all studies. Other standard eigen-solvers are also tested to ensure that the reported spurious solutions are not due to artifacts of a particular eigen-solver.

## 3.1. Non-spectral pollution spurious modes

We will demonstrate in this subsection that non-spectral pollution spurious modes occur when a severe one-sided finite difference approximation is employed, either in the asymmetric discretization of the differential equation, i.e., the OFD methods, or in the asymmetric boundary treatment of the CFD methods.

### 3.1.1. Spurious modes raised in OFD methods

We first consider two eigenvalue problems, i.e., the 1D Helmholtz equation with Dirichlet boundary conditions Eq. (31) and the simply supported beam Eq. (29). In these two examples, spurious solutions are found in OFD methods, but not in CFD methods.

The boundary conditions can be imposed analytically in the CFD method for these examples, because the eigenfunctions of these examples are sine functions. The sine functions with integer wavenumbers satisfy the anti-symmetry or skew-symmetry property at nodes $x = 0$ and $x = \pi$. Thus, the fictitious values outside $[0, \pi]$ can be attained through the so-called anti-symmetric extension [19,20]. No approximation error is involved in such an extension.

Therefore, boundary conditions are analytically satisfied in the present CFD discretizations, so that the PDE discretization scheme, i.e., the CFD here, will be fully responsible to the possible occurrence of spurious modes, if any.

For OFD methods, an analytical boundary closure is only feasible to the 1D Helmholtz equation. For example, the homogeneous Dirichlet boundary condition at $u = 0$ can be realized by setting non-diagonal elements of the first row of the discretized matrix as zero, while the diagonal element as one. Numerically, such an implementation introduces two trivial modes with their eigenvalues being one. These two boundary modes are not spurious solutions in the classical sense, and can be easily identified in practice. On the other hand, for the simply supported beam, boundary conditions can only be enforced approximately. These conditions will be imposed by using the boundary closure scheme 2, as discussed for free edges in Section 2.1.2. Both OFD1 and OFD2 discretizations will be considered.

It is found that, by using the same standard eigen-solver, spurious modes typically appear in OFD methods, but not in the CFD method. The relationship between the number of spurious modes and the kernel bandwidth $M$ is studied in Fig. 4. The CFD method is free of spurious solutions for any $M$ value, while similar polluted patterns are observed for the OFD methods in both examples. Note that in the simply supported beam case, by using the boundary closure scheme 2, the dimension of discrete matrix for both OFD1 and OFD2 is $(N - 4) \times (N - 4)$. Thus, when $N = 61$, there is no spurious mode with 57 real modes. Therefore, in both examples, both OFD1 and OFD2 do not deliver spurious modes when $M$ is as small as 2. For a larger $M = 4$ with the degree of asymmetry {0:8}, the OFD2 begins to produce spurious modes, and the first mode number of the lowest spurious mode is about 20–30. In other words, only the first 20 modes may be reliable. As $M$ increases, it is clear from Fig. 4 that the number of the non-spurious modes of the OFD2 decreases almost
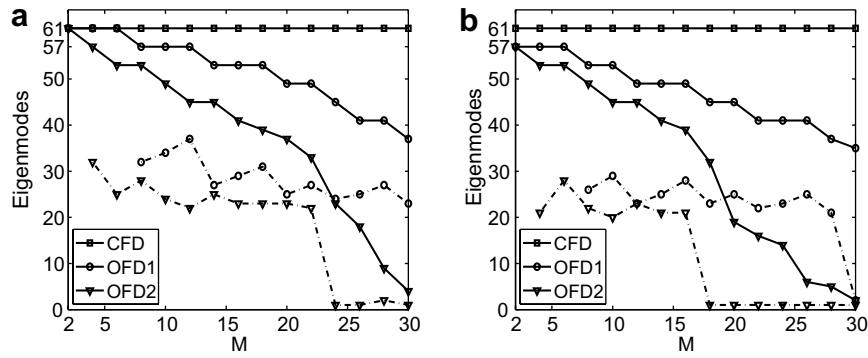
Fig. 4. Number of spurious modes against the kernel bandwidth $M$ with $N = 61$. (a) 1D Helmholtz equation with Dirichlet boundary conditions; (b) Simply supported beam. In both charts, solid line and dashed line show respectively the total number of real eigenmodes and the mode number of the lowest complex eigenmode.

linearly to just a few when $M = 30$. On the other hand, when $M$ is large, the fundamental mode is polluted too. Thus, the OFD2 eigenmode analysis becomes unreliable for $M \geqslant 24$. Similar pattern can be observed for the OFD1 method in Fig. 4. Spurious solutions appear at

$M = 8$ with the same degree of asymmetry {0:8}. Consequently, for a fixed $M$, it can be concluded from Fig. 4 that the OFD2 is more unstable than the OFD1.

We next show that the spurious modes of the OFD methods are non-spectral pollution in nature. This is tested

Table 1
Spectral pollution test of the OFD2 method with $M = 12$ for 1D Helmholtz equation with Dirichlet boundary conditions

| Mode | $k^2$ | $N = 41$ | | $N = 81$ | | $N = 161$ | |
|---|---|---|---|---|---|---|---|
| | | Re($k^2$) | Im($k^2$) | Re($k^2$) | Im($k^2$) | Re($k^2$) | Im($k^2$) |
| 1 | 1 | 1.0000 | 0.0 | 1.0000 | 0.0 | 1.0000 | 0.0 |
| 2 | 4 | 4.0000 | 0.0 | 4.0000 | 0.0 | 4.0000 | 0.0 |
| 3 | 9 | 9.0000 | 0.0 | 9.0000 | 0.0 | 9.0000 | 0.0 |
| 4 | 16 | 16.0000 | 0.0 | 16.0000 | 0.0 | 16.0000 | 0.0 |
| 5 | 25 | 25.0000 | 0.0 | 25.0000 | 0.0 | 25.0000 | 0.0 |
| 6 | 36 | 36.0000 | 0.0 | 36.0000 | 0.0 | 36.0000 | 0.0 |
| 7 | 49 | 49.0000 | 0.0 | 49.0000 | 0.0 | 49.0000 | 0.0 |
| 8 | 64 | 64.0000 | 0.0 | 64.0000 | 0.0 | 64.0000 | 0.0 |
| 9 | 81 | 81.0000 | 0.0 | 81.0000 | 0.0 | 81.0000 | 0.0 |
| 10 | 100 | 99.9991 | 0.0 | 100.0000 | 0.0 | 100.0000 | 0.0 |
| 11 | 121 | 120.9924 | 0.0 | 121.0000 | 0.0 | 121.0000 | 0.0 |
| 12 | 144 | 143.9970 | 0.0 | 144.0000 | 0.0 | 144.0000 | 0.0 |
| 13 | 169 | 169.4279 | 0.0 | 169.0000 | 0.0 | 169.0000 | 0.0 |
| 14 | 196 | 200.0808 | 0.0 | 196.0000 | 0.0 | 196.0000 | 0.0 |
| 15 | 225 | 230.7886 | 0.0 | 225.0000 | 0.0 | 225.0000 | 0.0 |
| 16 | 256 | 232.1581 | 12.3024 | 256.0000 | 0.0 | 256.0000 | 0.0 |
| 17 | 289 | 232.1581 | −12.3024 | 289.0000 | 0.0 | 289.0000 | 0.0 |
| 18 | 324 | 283.8241 | 0.0 | 324.0000 | 0.0 | 324.0000 | 0.0 |
| 19 | 361 | 279.7546 | −132.2395 | 360.9996 | 0.0 | 361.0000 | 0.0 |
| 20 | 400 | 279.7546 | 132.2395 | 399.9983 | 0.0 | 400.0000 | 0.0 |
| 21 | 441 | 280.0665 | −132.3642 | 440.9941 | 0.0 | 441.0000 | 0.0 |
| 22 | 484 | 280.0665 | 132.3642 | 483.9847 | 0.0 | 484.0000 | 0.0 |
| 23 | 529 | 364.6390 | 0.0 | 528.9735 | 0.0 | 529.0000 | 0.0 |
| 24 | 576 | 289.2068 | 356.9520 | 575.9939 | 0.0 | 576.0000 | 0.0 |
| 25 | 625 | 289.2068 | −356.9520 | 625.1713 | 0.0 | 625.0000 | 0.0 |
| 26 | 676 | 289.2073 | −356.9522 | 676.8378 | 0.0 | 676.0000 | 0.0 |
| 27 | 729 | 289.2073 | 356.9522 | 731.6995 | 0.0 | 729.0000 | 0.0 |
| 28 | 784 | 461.2474 | 0.0 | 791.1601 | 0.0 | 784.0000 | 0.0 |
| 29 | 841 | 568.8530 | 0.0 | 859.8901 | 0.0 | 841.0000 | 0.0 |
| 30 | 900 | 686.7150 | 0.0 | 920.5703 | −32.4314 | 900.0000 | 0.0 |
| 31 | 961 | 812.9487 | 0.0 | 920.5703 | 32.4314 | 961.0000 | 0.0 |
| 32 | 1024 | 154.5138 | −837.0814 | 936.1715 | 0.0 | 1024.0000 | 0.0 |
| 33 | 1089 | 154.5138 | 837.0814 | 964.2473 | 0.0 | 1089.0000 | 0.0 |
| 34 | 1156 | 154.5138 | −837.0814 | 1059.7287 | 0.0 | 1156.0000 | 0.0 |
| 35 | 1225 | 154.5138 | 837.0814 | 1149.2771 | 0.0 | 1225.0000 | 0.0 |

by varying the meshsize, with a fixed $M$. Only one OFD method is reported for each example, i.e., OFD1 with $M = 12$ for 1D Helmholtz equation and OFD2 with $M = 12$ for simply supported beam. See Tables 1 and 2. For both examples, the result for the other OFD method is similar. In both tables, by taking $N = 41$, 81, and 161, the first 35 numerical eigenvalues are listed together with analytical eigenvalues. It can be observed in Table 1 that by using $N = 41$, the first ten OFD2 eigenmodes roughly agree with the true ones. The numerical error becomes very large at the 15th mode, then spurious modes arrive at the 16th mode. Similarly, by using $N = 81$, the first 20 modes of the OFD2 are good, while the accuracy is lost at the 28th mode, with the 29th mode being spurious. In both cases, the first spurious mode occurs in the place where the numerical error is substantially large. The numerical modes after the spurious modes are simply useless as can be seen from the Table 1. Moreover, the spurious modes attained by using different meshsizes are clearly different. In other words, such modes are not possessed by the discrete OFD2 matrix, i.e., they are not spectral pollution.

By refining the mesh again to $N = 161$, the first 35 modes are then all physical as can be seen from Table 1, although the OFD2 still produces spurious modes later on. The similar non-spectral pollution pattern can also be observed in Table 2.

It is of great interest to study the origin of spurious modes in both OFD methods. Spectral pollution is usually due to the loss of certain constraints. Nevertheless, no necessary constraint is missing in the present OFD discretization. Thus, the cause of the non-spectral pollution spurious modes should be due to the severe asymmetric approximation. For the present two examples, the symmetric PDE discretization via the CFD methods is free of spurious solutions. For OFD methods, no matter whether boundary conditions are satisfied exactly or approximately, non-spectral pollution spurious solutions are generated. Thus, boundary closure methods are non-essential to non-spectral pollution spurious solutions. Consequently, it is the asymmetric approximation used in the PDE discretization that produces spurious modes. This can be further confirmed quantitatively. For example, it can be seen in

Table 2
Spectral pollution test of the OFD1 method with $M = 12$ in beam analysis with simply supported edges

| Mode | $k^2$ | $N = 41$ | | $N = 81$ | | $N = 161$ | |
|---|---|---|---|---|---|---|---|
| | | $Re(k^2)$ | $Im(k^2)$ | $Re(k^2)$ | $Im(k^2)$ | $Re(k^2)$ | $Im(k^2)$ |
| 1 | 1 | 1.0000 | 0.0 | 1.0000 | 0.0 | 1.0000 | 0.0 |
| 2 | 16 | 16.0000 | 0.0 | 16.0000 | 0.0 | 16.0000 | 0.0 |
| 3 | 81 | 81.0000 | 0.0 | 81.0000 | 0.0 | 81.0000 | 0.0 |
| 4 | 256 | 256.0000 | 0.0 | 256.0000 | 0.0 | 256.0000 | 0.0 |
| 5 | 625 | 625.0011 | 0.0 | 625.0000 | 0.0 | 625.0000 | 0.0 |
| 6 | 1296 | 1296.0194 | 0.0 | 1296.0000 | 0.0 | 1296.0000 | 0.0 |
| 7 | 2401 | 2401.1660 | 0.0 | 2401.0000 | 0.0 | 2401.0000 | 0.0 |
| 8 | 4096 | 4096.8462 | 0.0 | 4096.0001 | 0.0 | 4096.0000 | 0.0 |
| 9 | 6561 | 6563.7037 | 0.0 | 6561.0014 | 0.0 | 6561.0000 | 0.0 |
| 10 | 10000 | 10005.2813 | 0.0 | 10000.0090 | 0.0 | 10000.0000 | 0.0 |
| 11 | 14641 | 14648.5630 | 0.0 | 14641.0416 | 0.0 | 14641.0000 | 0.0 |
| 12 | 20736 | 20773.4306 | 0.0 | 20736.1550 | 0.0 | 20736.0000 | 0.0 |
| 13 | 28561 | 28858.6885 | 0.0 | 28561.4876 | 0.0 | 28560.9999 | 0.0 |
| 14 | 38416 | 40176.5950 | 0.0 | 38417.3281 | 0.0 | 38416.0000 | 0.0 |
| 15 | 50625 | 59272.1402 | 11429.9327 | 50628.1820 | 0.0 | 50625.0001 | 0.0 |
| 16 | 65536 | 59272.1402 | −11429.9327 | 65542.7681 | 0.0 | 65536.0010 | 0.0 |
| 17 | 83521 | 61381.1026 | 15881.6611 | 83533.8256 | 0.0 | 83521.0038 | 0.0 |
| 18 | 104976 | 61381.1026 | −15881.6611 | 104997.6224 | 0.0 | 104976.0115 | 0.0 |
| 19 | 130321 | 72970.9389 | 0.0 | 130353.2364 | 0.0 | 130321.0301 | 0.0 |
| 20 | 160000 | 107372.9000 | 0.0 | 160042.2431 | 0.0 | 160000.0720 | 0.0 |
| 21 | 194481 | 144701.1288 | 0.0 | 194530.6066 | 0.0 | 194481.1596 | 0.0 |
| 22 | 234256 | −67369.6886 | −165136.4465 | 234316.4814 | 0.0 | 234256.3326 | 0.0 |
| 23 | 279841 | −67369.6886 | 165136.4465 | 279950.0632 | 0.0 | 279841.6575 | 0.0 |
| 24 | 331776 | −67369.6886 | −165136.4465 | 332073.7936 | 0.0 | 331777.2401 | 0.0 |
| 25 | 390625 | −67369.6886 | 165136.4465 | 391492.6247 | 0.0 | 390627.2423 | 0.0 |
| 26 | 456976 | 190943.5739 | 0.0 | 459288.7211 | 0.0 | 456979.9007 | 0.0 |
| 27 | 531441 | 248396.3089 | 0.0 | 537023.7537 | 0.0 | 531447.5468 | 0.0 |
| 28 | 614656 | 319126.2592 | 0.0 | 627203.7524 | 0.0 | 614666.6240 | 0.0 |
| 29 | 707281 | 405131.7410 | 0.0 | 734788.9759 | 0.0 | 707297.6984 | 0.0 |
| 30 | 810000 | 508164.4227 | 0.0 | 873978.1427 | 0.0 | 810025.4541 | 0.0 |
| 31 | 923521 | 629373.0778 | 0.0 | 975532.2594 | −223197.1993 | 923558.6657 | 0.0 |
| 32 | 1048576 | 768815.8817 | 0.0 | 975532.2594 | 223197.1993 | 1048630.1383 | 0.0 |
| 33 | 1185921 | 924562.9945 | 0.0 | 979142.0480 | 226010.3757 | 1185996.6065 | 0.0 |
| 34 | 1336336 | 1090814.8570 | 0.0 | 979142.0480 | −226010.3757 | 1336438.5885 | 0.0 |
| 35 | 1500625 | 1255396.7567 | 0.0 | 1075573.4963 | 0.0 | 1500760.2002 | 0.0 |

Fig. 4 that spurious solutions appear at the same degree of asymmetry {0:8} for both the OFD1 and OFD2 approaches. In fact, Fig. 4 illustrates the dependence of the occurrence of spurious modes on the degree of the asymmetric approximation associated with $M$.

### 3.1.2. Spurious modes raised in CFD and OFD schemes

We next examine spurious modes raised in the CFD scheme of free-edged beam Eq. (30). The previous studies suggest that in order to avoid non-spectral pollution spurious modes, high-order central finite difference methods should be employed in PDE discretizations. However, due to complex boundary conditions involved in the free-edged beams, a fictitious domain boundary method without involving one-sided approximations is unavailable. Thus, the MIB boundary method which employs a one-sided approximation in determining fictitious values has to be utilized. Note that based on the MIB boundary method, the symmetric CFD is used in the PDE discretization.

The MIB boundary method presented in the last section can be easily modified for the present example. In particular, since there are two boundary conditions in Eq. (30) at each end, one can solve two fictitious values at first step or at any iteration step. Thus, we usually take both $M$ and $L$ to be even integers. To estimate $M$ fictitious values, $M/2$ steps MIB iteration will be enough [25].

With its degree of asymmetry being {2:L}, the MIB method may yield spurious modes when $L$ is large, see Fig. 5a. It can be seen that the CFD-MIB method is free of spurious solutions when $L \leqslant 12$. When the degree of asymmetry is {2:14}, the CFD-MIB method yields spurious modes for all tested $M$ vales. The spurious solutions of three different $M$ values are almost the same until $L$ is as large as 24. When $L > 24$, a smaller $M$, such as $M = 10$, produce a slightly better results than other $M$ values. These results suggest that in the MIB method, a spurious solution is due to the use of a large $L$, but not $M$. Moreover, for a stable computation free of spurious solutions, one should choose $L \leqslant 12$ in the MIB boundary method. This is further confirmed in Fig. 5b, in which

the CFD-MIB method with $L = 12$ does not suffer from the spurious solutions at all, while both OFD approaches produce spurious modes. For this example, the critical degree of asymmetry for OFD approaches is {0:8}, i.e., OFD1 with $M = 8$ and OFD2 with $M = 4$. We finally note that although $L$ is restricted to be not greater than 12, the MIB method is designed in a stable manner to generate enough fictitious points for $M > 12$.

The spectral pollution test of the CFD-MIB method with $M = L = 14$ is considered in Table 3. For $N = 41$ and $N = 81$, first 30 modes and modes No. 25 to No. 54 are shown, respectively. It is clear that as in previous examples, these spurious solutions are non-spectral pollution ones. They are due to the severe asymmetric approximation introduced by a large $L$ in the MIB boundary treatment, although the symmetric CFD approximation is still used in the PDE discretization. The spectral pollution tests of both OFD approaches are similar to those presented in the previous examples, are thus omitted here.

The present results also indicate that the occurrence frequency of spurious modes in the CFD-MIB discretization is lower than that in the OFD discretization. For the present example, the critical value of the stable OFD1 is $M = 8$, while that of the CFD-MIB is $L = 12$. This actually means that the CFD-MIB method has a much wider range of parameters to guarantee the stability than the OFD approaches. This stability property may be explained based on two considerations. First, the MIB method involves the asymmetric approximation only in fictitious values, while the OFD approaches use asymmetric approximations in the PDE discretization. Thus, unlike in OFD approaches, there is only some indirect effect of non-symmetric approximations on the final CFD-MIB discrete matrix. Moreover, such an effect is further balanced by the symmetric finite difference approximation to the PDE. Second, the degree of asymmetry of the MIB and OFD1 is, respectively, {2:L} and {0:M}. Thus, a completely one-sided approximation is used in the OFD approaches, while a partially one-sided approximation is used in the MIB method. As a consequence, the MIB is stable on a larger parameter space.
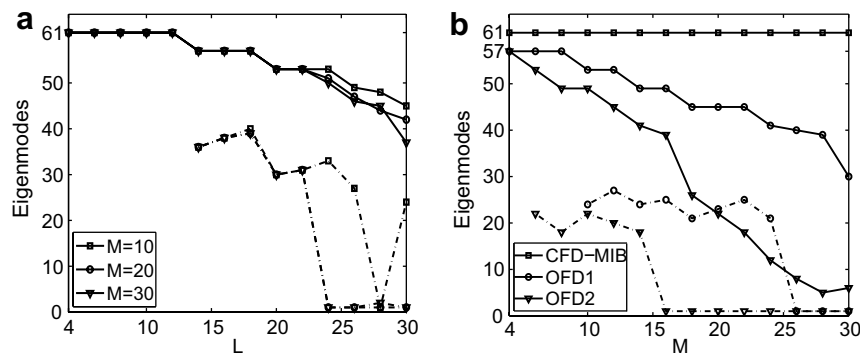


Fig. 5. Spurious mode studies of free-edged beam with $N = 61$. In both charts, the solid line and dashed line show respectively the total number of real eigenmodes and the mode number of the lowest complex eigenmode. In (a), three $M$ values are considered for the CFD-MIB method; In (b), $L = 12$ in the CFD-MIB method.

Table 3
Spectral pollution test of the CFD-MIB method with $M = L = 14$ in beam analysis with free edges

| Mode | $N = 41$ | | | Mode | $N = 81$ | | |
|---|---|---|---|---|---|---|---|
| | $k^2$ | Re($k^2$) | Im($k^2$) | | $k^2$ | Re($k^2$) | Im($k^2$) |
| 1 | 5.1388 | 5.1388 | 0.0 | 25 | 422825.0625 | 422803.2054 | 0.0 |
| 2 | 39.0470 | 39.0470 | 0.0 | 26 | 493155.0625 | 493090.2614 | 0.0 |
| 3 | 150.0643 | 150.0643 | 0.0 | 27 | 571914.0625 | 571761.3644 | 0.0 |
| 4 | 410.0623 | 410.0623 | 0.0 | 28 | 659750.0625 | 659435.0733 | 0.0 |
| 5 | 915.0625 | 915.0625 | 0.0 | 29 | 757335.0625 | 756745.5164 | 0.0 |
| 6 | 1785.0625 | 1785.0626 | 0.0 | 30 | 865365.0625 | 864347.7892 | 0.0 |
| 7 | 3164.0625 | 3164.0640 | 0.0 | 31 | 984560.0625 | 982930.9521 | 0.0 |
| 8 | 5220.0625 | 5220.0759 | 0.0 | 32 | 1115664.0625 | 1113241.2517 | 0.0 |
| 9 | 8145.0625 | 8145.1370 | 0.0 | 33 | 1259445.0625 | 1256116.1239 | 0.0 |
| 10 | 12155.0625 | 12155.3228 | 0.0 | 34 | 1416695.0625 | 1412525.4623 | 0.0 |
| 11 | 17490.0625 | 17490.4728 | 0.0 | 35 | 1588230.0625 | 1583611.8032 | 0.0 |
| 12 | 24414.0625 | 24412.7393 | 0.0 | 36 | 1774890.0625 | 1770718.7067 | 0.0 |
| 13 | 33215.0625 | 33202.3865 | 0.0 | 37 | 1977539.0625 | 1975400.1143 | 0.0 |
| 14 | 44205.0625 | 44150.7470 | 0.0 | 38 | 2197065.0625 | 2199413.1365 | 0.0 |
| 15 | 57720.0625 | 57558.4101 | 0.0 | 39 | 2434380.0625 | 2444708.3396 | 0.0 |
| 16 | 74120.0625 | 73763.2842 | 0.0 | 40 | 2690420.0625 | 2713439.9401 | 0.0 |
| 17 | 93789.0625 | 93231.2941 | 0.0 | 41 | 2966145.0625 | 3008023.0214 | 0.0 |
| 18 | 117135.0625 | 116705.3480 | 0.0 | 42 | 3262539.0625 | 3331272.9065 | 0.0 |
| 19 | 144590.0625 | 145344.3685 | 0.0 | 43 | 3580610.0625 | 3686686.1384 | 0.0 |
| 20 | 176610.0625 | 180833.8300 | 0.0 | 44 | 3921390.0625 | 4078980.4787 | 0.0 |
| 21 | 213675.0625 | 225755.9334 | 0.0 | 45 | 4285935.0625 | 4515106.7843 | 0.0 |
| 22 | 256289.0625 | 285688.6601 | 0.0 | 46 | 4675325.0625 | 5005865.8925 | 0.0 |
| 23 | 304980.0625 | 382328.2239 | 0.0 | 47 | 5090664.0625 | 5566212.1380 | 0.0 |
| 24 | 360300.0625 | 371344.5844 | 110553.9941 | 48 | 5533080.0625 | 5950670.7882 | −1739324.7008 |
| 25 | 422825.0625 | 371344.5844 | −110553.9941 | 49 | 6003725.0625 | 5950670.7882 | 1739324.7008 |
| 26 | 493155.0625 | 372600.0093 | −106568.6485 | 50 | 6503775.0625 | 5950682.9110 | 1739573.2638 |
| 27 | 571914.0625 | 372600.0093 | 106568.6485 | 51 | 7034430.0625 | 5950682.9110 | −1739573.2638 |
| 28 | 659750.0625 | 506889.2291 | 0.0 | 52 | 7596914.0625 | 6203210.4564 | 0.0 |
| 29 | 757335.0625 | 624060.7981 | 0.0 | 53 | 8192475.0625 | 6892089.8700 | 0.0 |
| 30 | 865365.0625 | 747753.7921 | 0.0 | 54 | 8822385.0625 | 7602542.4464 | 0.0 |

On the other hand, following the same two considerations, the CFD-MIB method is more accurate than the OFD approaches. First, the central finite difference approximations will be more accurate than the one-sided finite difference approximations in PDE discretization level. Second, partially symmetric approximations are better than completely one-sided approximations. Moreover, a larger $L$ and arbitrarily large $M$ are allowed in the CFD-MIB method to deliver higher-order accuracy. Therefore, the CFD-MIB method can attain higher order of accuracy than the OFD approaches. In fact, in previous calculations, orders of accuracy up to 12, sometimes even 16, have been attained by the MIB method [22,23,26,24].

The high accuracy of the CFD-MIB method is demonstrated in Fig. 6 for the present eigenvalue problem. As shown in Fig. 6a and b, the CFD-MIB method is more accurate than both OFD approaches in estimating the first 30 eigenmodes, no matter a small or large bandwidth $M$ is employed. In terms of estimating the fundamental mode, the CFD-MIB method still attains the highest accuracy by varying either meshsize $N$ or bandwidth $M$, see Fig. 6c and d. On the other hand, a comparison between two OFD approaches suggests that the OFD2 is usually more accurate than the OFD1 when $M$ is small. However, as shown in Fig. 6b and d, when $M$ is large, the OFD2

accuracy deteriorates quickly due to the instability, so that the OFD1 becomes more accurate.

### 3.2. Spectral pollution spurious modes

We next study spectral pollution by considering 1D Helmholtz equation Eq. (32) and 2D Helmholtz equation Eq. (33) with Neumann boundary conditions. Spectral pollution is found in OFD methods for the 2D Helmholtz equation, but not for the 1D one.

#### 3.2.1. Spurious modes in solving the 1D Helmholtz equation
The 1D Helmholtz equation Eq. (32) is studied first. For the CFD approach, the MIB boundary method is similarly formulated as in the free-edged beam analysis. Based on the Neumann boundary condition $u' = 0$, it can be further derived from the Helmholtz equation that $u''' = 0$. Two boundary conditions are employed in the MIB boundary treatment. By considering $L = 10$, and $M$ ranging from 4 to 30, the CFD-MIB produces all real eigenvalues, i.e., free of spurious solutions, see Fig. 7.

The difference between the present problem and the free-edged beam is that now one can make use of both boundary closure schemes 1 and 2 of Section 2.1.2 for OFD approaches. We consider both boundary closure schemes
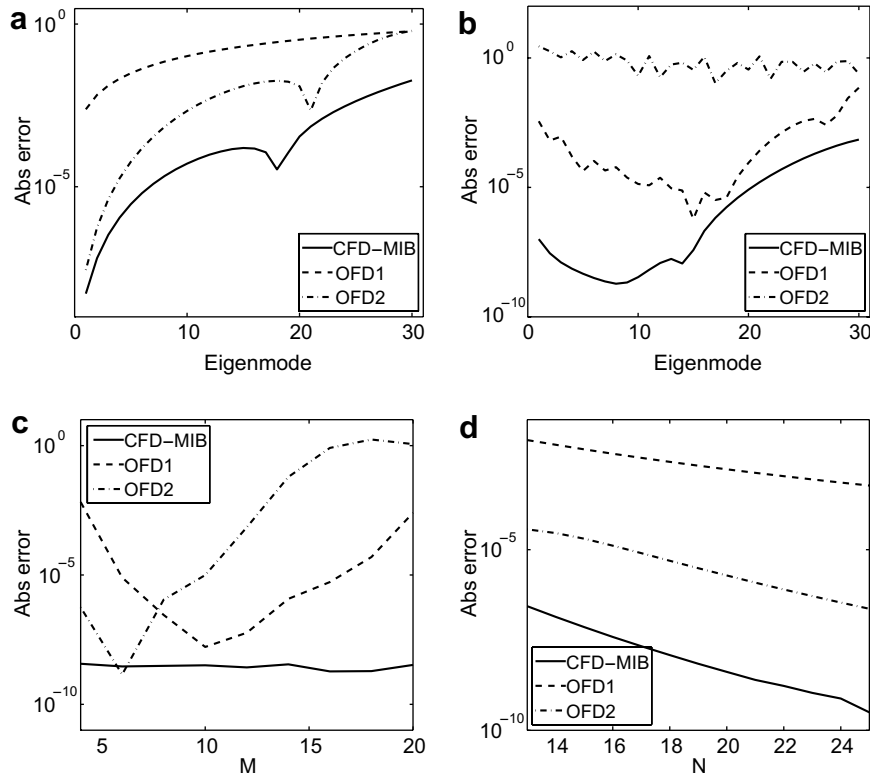
Fig. 6. Accuracy comparisons of the free-edged beam analysis. (a) Absolute errors in first 30 eigenmodes with $M = 4$, $N = 61$, and $L = 4$. (b) Absolute errors in first 30 eigenmodes with $M = 20$, $N = 61$, and $L = 12$. (c) Absolute errors in the fundamental eigenmode against meshsize $N$ with $M = 6$ and $L = 10$. (d) Absolute errors in the fundamental eigenmode against bandwidth $M$ with $N = 61$ and $L = 6$.
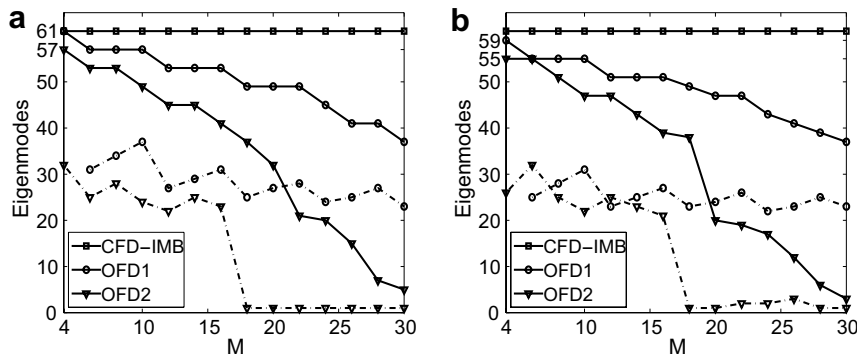


Fig. 7. Spurious mode study of the 1D Helmholtz equation with $N = 61$ and $L = 10$. The solid line and dashed line show respectively the total number of real eigenmodes and the mode number of the lowest complex eigenmode. The boundary closure schemes 1 and 2 of Section 2.1.2 is used, respectively, in (a) and (b) for both OFD methods.

in Fig. 7. We note that the matrix dimension by using the OFD2 is $(N - 1) \times (N - 1)$ in this case. Thus, with $N = 61$ in Fig. 7, by producing 59 real eigenvalues, the OFD2 is actually stable when $M = 4$. Except for the difference in dimension, it can be observed from Fig. 7 that the spurious mode patterns of OFD methods with closure scheme 1 or scheme 2 are quite similar.

The spectral pollution tests are considered for both OFD1 and OFD2 with both closure schemes 1 and 2. The results of these four tests are similar. For simplicity,

we only present OFD2 results with the closure scheme 1 in Table 4. These spurious modes are clearly non-spectral pollution ones.

### 3.2.2. Spurious modes in solving the 2D Helmholtz equation

However, spectral pollution is found in the OFD methods for the 2D Helmholtz equation with Neumann boundary conditions, Eq. (33). In particular, it is found that lots of spurious modes occur by using the boundary closure scheme 1 of Section 2.1.2, while these modes can be

Table 4
Spectral pollution test of the OFD2 method with boundary closure scheme 1 and $M = 10$ for 1D Helmholtz equation with Neumann boundary conditions

| Mode | $k^2$ | $N = 26$ | | $N = 51$ | | $N = 101$ | |
|---|---|---|---|---|---|---|---|
| | | $Re(k^2)$ | $Im(k^2)$ | $Re(k^2)$ | $Im(k^2)$ | $Re(k^2)$ | $Im(k^2)$ |
| 1 | 1 | 1.0000 | 0.0 | 1.0000 | 0.0 | 1.0000 | 0.0 |
| 2 | 4 | 4.0000 | 0.0 | 4.0000 | 0.0 | 4.0000 | 0.0 |
| 3 | 9 | 9.0000 | 0.0 | 9.0000 | 0.0 | 9.0000 | 0.0 |
| 4 | 16 | 16.0000 | 0.0 | 16.0000 | 0.0 | 16.0000 | 0.0 |
| 5 | 25 | 25.0000 | 0.0 | 25.0000 | 0.0 | 25.0000 | 0.0 |
| 6 | 36 | 36.0003 | 0.0 | 36.0000 | 0.0 | 36.0000 | 0.0 |
| 7 | 49 | 48.9880 | 0.0 | 49.0000 | 0.0 | 49.0000 | 0.0 |
| 8 | 64 | 63.7428 | 0.0 | 64.0000 | 0.0 | 64.0000 | 0.0 |
| 9 | 81 | 80.8239 | 0.0 | 81.0000 | 0.0 | 81.0000 | 0.0 |
| 10 | 100 | 98.9910 | 19.6053 | 100.0000 | 0.0 | 100.0000 | 0.0 |
| 11 | 121 | 98.9910 | −19.6053 | 121.0002 | 0.0 | 121.0000 | 0.0 |
| 12 | 144 | 106.7989 | −22.4931 | 144.0008 | 0.0 | 144.0000 | 0.0 |
| 13 | 169 | 106.7989 | 22.4931 | 168.9996 | 0.0 | 169.0000 | 0.0 |
| 14 | 196 | 116.5843 | 103.8043 | 195.9781 | 0.0 | 196.0000 | 0.0 |
| 15 | 225 | 116.5843 | −103.8043 | 224.8563 | 0.0 | 225.0000 | 0.0 |
| 16 | 256 | 124.0506 | 99.9955 | 255.4612 | 0.0 | 256.0000 | 0.0 |
| 17 | 289 | 124.0506 | −99.9955 | 287.8351 | 0.0 | 289.0000 | 0.0 |
| 18 | 324 | 169.7701 | 0.0 | 323.4844 | 0.0 | 324.0000 | 0.0 |
| 19 | 361 | 295.5964 | 0.0 | 367.9723 | 0.0 | 361.0000 | 0.0 |
| 20 | 400 | 92.0373 | −282.5523 | 407.2723 | 82.9183 | 400.0001 | 0.0 |

avoided by using the closure scheme 2. By using the boundary closure scheme 1, the first 40 eigenvalues estimated by the both OFD approaches are listed in Table 5. It can be observed from Table 5 that most of the numerical eigenmodes are unrelated to the true spectrum. Moreover, they are actually the spectral pollution modes, in the sense that these modes converge by refining the mesh, and persist no matter that either OFD1 or OFD2 is used. It is noted that spectral pollution modes here have zero imaginary parts. Thus, in practice, it is computationally challenging to distinguish these spurious modes from the true eigenmodes. For example, there are only three correct eigenmodes, i.e., the 8th, 21st and 22nd mode, indistinguishably interspersed among 19 spectral pollution modes in the first 22 numerical modes. On the other hand, it is interesting to observe that the OFD2 also produces non-spectral pollution spurious modes which have non-zero imaginary parts and do not converge after refining the mesh. Furthermore, besides the co-existence of two types of spurious modes, it is also found that many true eigenvalues are simply missed in the numerical spectrum by using the boundary closure scheme 1. However, by using the boundary closure scheme 2 of Section 2.1.2, the spurious modes of two OFD approaches will be only the non-spectral pollution ones. The existence of the spectral pollution modes and the absence of many true eigenmodes are not observed in results of the closure scheme 2. The results of the boundary closure scheme 2 are similar to those in the previous sections, and are omitted here.

It is of great interest to study the cause of the spectral pollution modes in the boundary closure scheme 1 of Section 2.1.2. According to the literature results, it should be due to the loss of constraint in the numerical discretization. For the boundary closure scheme 2 of Section 2.1.2, the governing PDE is discretized at each point, while the boundary condition has been naturally incorporated into such a discretization. In other words, at each grid node near boundaries, both the PDE and boundary conditions are properly accounted. However, this is not the case for the boundary closure scheme 1. In the boundary closure scheme 1, at boundary nodes, only boundary conditions are discretized. The information contained in the PDE is not included. This may not be critical in 1D, but would cause significant problem in higher dimensions. For example, along the boundary $\Gamma_1 = \{(x,y)|x = 0\}$, the algebraic equations for all boundary nodes are the same, because they are all discretized from the same Neumann boundary condition along the $x$ direction. However, in 2D, the true eigenfunctions are generally not a constant, instead they may fluctuate along the $y$ direction on $\Gamma_1$. Such a fluctuation indicated by the governing PDE is clearly missing in the boundary closure scheme 1. The loss of such a constraint creates eigensolution sub-space. Thus, the discrete matrix possess the spectral pollution spurious modes. This perhaps explains why the boundary closure scheme 1 in 2D has spectral pollution, but it does not in 1D. Nevertheless, we note finally that the absence of many true eigenmodes in 2D is still unaccountable. More detailed theoretical and computational studies are needed for this spurious solution problem.

The spurious mode study of the CFD-MIB method and the OFD methods with boundary closure scheme 2 of Section 2.1.2 is given in Fig. 8. For the MIB method, two boundary conditions at each end are used as in the 1D case. The CFD-MIB is found to be free of spurious solutions in 2D, see Fig. 8. By using the boundary closure scheme 2, the matrix dimension of both OFD approaches is $(N − 1)^2 \times (N − 1)^2$. Thus, by attaining 1521 real modes, both

Table 5
Spectral pollution test of the boundary closure scheme 1 for the 2D Helmholtz equation with Neumann boundary conditions. In both OFD approaches, we have $M = 4$

| Mode | $k^2$ | OFD1 | | | | OFD2 | | | |
|---|---|---|---|---|---|---|---|---|---|
| | | $N = 21$ | | $N = 41$ | | $N = 21$ | | $N = 41$ | |
| | | $\mathrm{Re}(k^2)$ | $\mathrm{Im}(k^2)$ | $\mathrm{Re}(k^2)$ | $\mathrm{Im}(k^2)$ | $\mathrm{Re}(k^2)$ | $\mathrm{Im}(k^2)$ | $\mathrm{Re}(k^2)$ | $\mathrm{Im}(k^2)$ |
| 1 | 1 | −0.5000 | 0.0 | −0.5000 | 0.0 | −0.5000 | 0.0 | −0.5000 | 0.0 |
| 2 | 1 | 0.6189 | 0.0 | 0.6180 | 0.0 | 0.6180 | 0.0 | 0.6180 | 0.0 |
| 3 | 2 | 0.6189 | 0.0 | 0.6180 | 0.0 | 0.6180 | 0.0 | 0.6180 | 0.0 |
| 4 | 4 | 1.5607 | 0.0 | 1.5615 | 0.0 | 1.5615 | 0.0 | 1.5616 | 0.0 |
| 5 | 4 | 1.5607 | 0.0 | 1.5615 | 0.0 | 1.5615 | 0.0 | 1.5616 | 0.0 |
| 6 | 5 | −1.6165 | 0.0 | −1.6179 | 0.0 | −1.6180 | 0.0 | −1.6180 | 0.0 |
| 7 | 5 | −1.6165 | 0.0 | −1.6179 | 0.0 | −1.6180 | 0.0 | −1.6180 | 0.0 |
| 8 | 8 | 2.0000 | 0.0 | 2.0000 | 0.0 | 2.0000 | 0.0 | 2.0000 | 0.0 |
| 9 | 9 | 2.5329 | 0.0 | 2.5408 | 0.0 | 2.5410 | 0.0 | 2.5414 | 0.0 |
| 10 | 9 | 2.5329 | 0.0 | 2.5408 | 0.0 | 2.5410 | 0.0 | 2.5414 | 0.0 |
| 11 | 10 | −2.5507 | 0.0 | −2.5607 | 0.0 | −2.5614 | 0.0 | −2.5616 | 0.0 |
| 12 | 10 | −2.5507 | 0.0 | −2.5607 | 0.0 | −2.5614 | 0.0 | −2.5616 | 0.0 |
| 13 | 13 | 3.4939 | 0.0 | 3.5282 | 0.0 | 3.5278 | 0.0 | 3.5311 | 0.0 |
| 14 | 13 | 3.4939 | 0.0 | 3.5282 | 0.0 | 3.5278 | 0.0 | 3.5311 | 0.0 |
| 15 | 16 | −3.4988 | 0.0 | −3.5376 | 0.0 | −3.5396 | 0.0 | −3.5414 | 0.0 |
| 16 | 16 | −3.4988 | 0.0 | −3.5376 | 0.0 | −3.5396 | 0.0 | −3.5414 | 0.0 |
| 17 | 17 | −4.4161 | 0.0 | 4.5155 | 0.0 | 4.5126 | 0.0 | 4.5248 | 0.0 |
| 18 | 17 | −4.4161 | 0.0 | 4.5155 | 0.0 | 4.5126 | 0.0 | 4.5248 | 0.0 |
| 19 | 18 | 4.4174 | 0.0 | −4.5198 | 0.0 | −4.5212 | 0.0 | −4.5310 | 0.0 |
| 20 | 20 | 4.4174 | 0.0 | −4.5198 | 0.0 | −4.5212 | 0.0 | −4.5310 | 0.0 |
| 21 | 20 | 4.9999 | 0.0 | 5.0000 | 0.0 | 5.0000 | 0.0 | 5.0000 | 0.0 |
| 22 | 25 | 4.9999 | 0.0 | 5.0000 | 0.0 | 5.0000 | 0.0 | 5.0000 | 0.0 |
| 23 | 25 | −5.2778 | 0.0 | 5.4971 | 0.0 | −5.4915 | 0.0 | 5.5201 | 0.0 |
| 24 | 25 | −5.2778 | 0.0 | 5.4971 | 0.0 | −5.4915 | 0.0 | 5.5201 | 0.0 |
| 25 | 25 | 5.2785 | 0.0 | −5.4977 | 0.0 | 5.5038 | 0.0 | −5.5244 | 0.0 |
| 26 | 26 | 5.2785 | 0.0 | −5.4977 | 0.0 | 5.5038 | 0.0 | −5.5244 | 0.0 |
| 27 | 26 | 6.0513 | 0.0 | −6.4652 | 0.0 | −6.4511 | 0.0 | 6.5156 | 0.0 |
| 28 | 29 | 6.0513 | 0.0 | −6.4652 | 0.0 | −6.4511 | 0.0 | 6.5156 | 0.0 |
| 29 | 29 | −6.0655 | 0.0 | 6.4681 | 0.0 | 6.5644 | 0.0 | −6.5189 | 0.0 |
| 30 | 32 | −6.0655 | 0.0 | 6.4681 | 0.0 | 6.5644 | 0.0 | −6.5189 | 0.0 |
| 31 | 34 | 6.7104 | 0.0 | −7.4166 | 0.0 | −7.4497 | 0.0 | 7.5097 | 0.0 |
| 32 | 34 | 6.7104 | 0.0 | −7.4166 | 0.0 | −7.4497 | 0.0 | 7.5097 | 0.0 |
| 33 | 36 | −6.7610 | 0.0 | 7.4231 | 0.0 | 8.0000 | 0.0 | −7.5126 | 0.0 |
| 34 | 36 | −6.7610 | 0.0 | 7.4231 | 0.0 | 8.1169 | 0.0 | −7.5126 | 0.0 |
| 35 | 37 | 7.2838 | 0.0 | 8.0000 | 0.0 | 8.1169 | 0.0 | 8.0000 | 0.0 |
| 36 | 37 | 7.2838 | 0.0 | −8.3468 | 0.0 | 8.1809 | −0.5217 | 8.5007 | 0.0 |
| 37 | 40 | −7.3442 | 0.0 | −8.3468 | 0.0 | 8.1809 | 0.5217 | 8.5007 | 0.0 |
| 38 | 40 | −7.3442 | 0.0 | 8.3569 | 0.0 | 8.1809 | −0.5217 | −8.5035 | 0.0 |
| 39 | 41 | −7.8417 | 0.0 | 8.3569 | 0.0 | 8.1809 | 0.5217 | −8.5035 | 0.0 |
| 40 | 41 | −7.8417 | 0.0 | −9.2509 | 0.0 | 8.4651 | −2.1190 | 9.4876 | 0.0 |
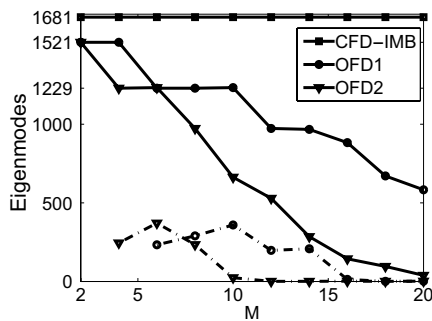


Fig. 8. Spurious mode study of the 2D Helmholtz equation with $N^2 = 41^2$ and $L = 10$. The solid line and dashed line show respectively the total number of real eigenmodes and the mode number of the lowest complex eigenmode.

approaches are stable when $M = 2$. We note that the fundamental mode is polluted in 2D when $M = 10$ and $M = 16$, respectively, for the OFD2 method and the OFD1 method. Such $M$ values are less than the counterparts in 1D. Thus, the instability issue of the OFD approaches seems to be more serious in higher dimensions.

The accuracy comparisons of three high-order finite difference methods are considered in Fig. 9. The OFD2 is more accurate than the OFD1 when $M$ is small in terms of both fundamental and high-frequency modes. However, when $M$ increases, the OFD1 will dominate the OFD2 due to the instability. In all cases, the CFD-MIB method is the most accurate finite difference method employing the same stencil length.
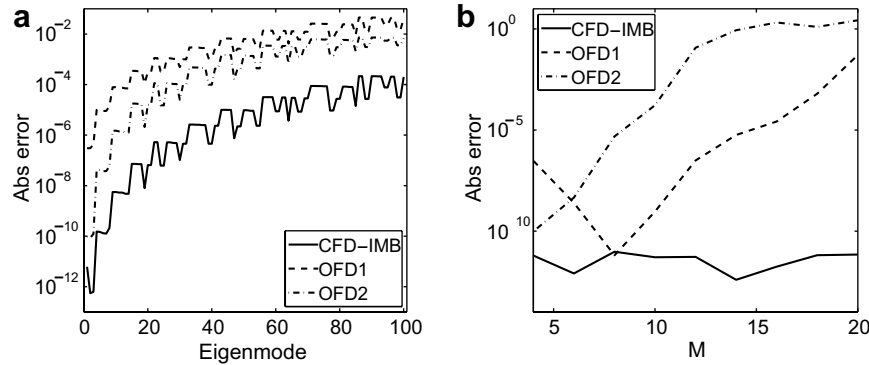
Fig. 9. Numerical accuracy comparisons of the 2D Helmholtz equation. (a) Absolute errors in first 100 eigenmodes with $M = 4$, $N^2 = 41^2$, and $L = 6$. (b) Absolute errors in the fundamental eigenmode against bandwidth $M$ with $N^2 = 41^2$ and $L = 6$.

## 4. Conclusion

In this work, the occurrence of spurious solutions of high-order finite difference methods is studied. High-order finite difference discretization of partial differential equations (PDEs) can be realized in two ways; One is to adopt one-sided approximations near the boundaries and the other maintains the use of a single central finite difference kernel by constructing fictitious domains outside the boundaries. For the one-sided finite difference (OFD) case, two typical matrix structures are considered, albeit the consideration of other matrix structures is possible. For both OFD approaches, two different boundary closure schemes are examined. For the central finite difference (CFD) case, boundary treatments free of one-sided approximations are only feasible for simple boundary conditions. To accommodate general boundary conditions, the matched interface and boundary (MIB) method has to be employed, in which one-sided approximations are involved in estimating fictitious domain values. Five prototype eigenvalue problems governed by different PDEs and boundary conditions in either one (1D) or two dimensions (2D) are utilized to study the stability and accuracy of various high-order finite difference methods. The origins of two types of spurious solutions, i.e., spectral pollution and non-spectral pollution, are investigated.

Non-spectral pollution spurious modes are found when severe asymmetric approximations are involved in the numerical discretization. For simple boundary conditions, such as the homogeneous Dirichlet ones in the 1D Helmholtz equation and the simply supported beam, analytical boundary closure method is available to form a translation invariant CFD discretization. Such a discretization is found to be free of spurious modes. However, based on a uniform mesh, OFD discretizations for these two examples generate spurious solutions, no matter whether the boundary conditions are satisfied analytically or approximately. These numerical studies suggest that non-spectral pollution spurious modes are due to the severe asymmetric approximation of the high-order OFD methods. In fact, such spurious solutions are generated by the OFD methods for all

tested examples. Moreover, these spurious solutions do not converge when the grid is refined, which means that they are non-spectral pollution spurious modes. Non-spectral pollution spurious solutions do not appear in the CFD-MIB method except the asymmetric approximation in the fictitious value determination of the MIB boundary scheme is severe, i.e., when $L > 12$.

Spectral pollution spurious modes are found in the OFD methods with the boundary closure scheme 1 of Section 2.1.2. Moreover, such spurious modes are generated in 2D but not 1D eigenvalue problems, governed by the same differential equation and boundary conditions, and discretized in the same way. The co-existence of both spectral pollution and non-spectral pollution has been observed. The spectral pollution spurious solutions are generally due to the loss of constraint in the mathematical modeling or numerical discretization. For the present case, some solution properties, such as the fluctuation along the tangential direction at the boundary, are not properly accounted in the boundary closure scheme 1. However, spectral pollution is not found in the OFD approaches with the boundary closure scheme 2 of Section 2.1.2 and the CFD-MIB method.

A comparison of high-order finite difference methods based on the present studies is in order. For the purpose of a comparison, when one scheme is less likely to produce spurious modes than another, the former will be said to be more stable than the latter. First, a comparison between two typical OFD approaches considered in this work (see Fig. 1) shows that the type 2 OFD method is more accurate, but is more unstable than the type 1 OFD method. Second, the present studies suggest a general rule that a central approximation instead of an asymmetric one should always be used if possible. This actually motivates the development of the matched interface and boundary (MIB) method to accommodate general boundary conditions for a translation invariant CFD discretization. The MIB method iteratively enforces the boundary conditions to generate accurate estimates of function values on a fictitious domain outside the boundary. Although one-sided interpolations are involved in the MIB iteration, we found

that the CFD-MIB method is more stable than the OFD approaches due to its use of CFD discretizations. Due to the stability, it is possible to design higher-order finite difference discretizations of PDEs, such as 12th or 16th order ones, with the CFD-MIB method. Consequently, the CFD-MIB method is not only more stable but also more accurate and efficient than the conventional OFD approaches.

## Acknowledgement

## References

[1] G. Bao, G.W. Wei, S. Zhao, Local spectral time-domain method for electromagnetic wave propagation, Opt. Lett. 28 (2003) 513–515.

[2] A. Bermudez, R. Duran, M.A. Muschietti, R. Rodriguez, J. Solomin, Finite element vibration analysis of fluid–solid systems without spurious modes, SIAM J. Numer. Anal. 32 (1995) 1280–1295.

[3] D. Boffi, F. Brezzi, L. Gastaldi, On the problem of spurious eigenvalues in the approximation of linear elliptic problems in mixed form, Math. Comput. 229 (1999) 121–140.

[4] D. Boffi, P. Fernandes, L. Gastaldi, I. Perugia, Computational models of electromagnetic resonators: analysis of edge element approximation, SIAM J. Numer. Anal. 36 (1999) 1264–1290.

[5] X. Cartoixa, D.Z.Y. Ting, T.C. McGill, Numerical spurious solutions in the effective mass approximation, J. Appl. Phys. 93 (2003) 3974–3981.

[6] J.T. Chen, S.Y. Lin, K.H. Chen, I.L. Chen, Mathematical analysis and numerical study of true and spurious eigenequations for free vibration of plates using real-part BEM, Comput. Mech. 34 (2004) 165–180.

[7] J.T. Chen, T.W. Lin, K.H. Chen, S.W. Chyuan, True and spurious eigensolutions for the problems with the mixed-type boundary conditions using BEMs, Finite Elements Anal. Des. 40 (2004) 1521–1549.

[8] E.B. Davies, M. Plum, Spectral pollution, IMA J. Numer. Anal. 24 (2004) 417–438.

[9] B.A. Foreman, Elimination of spurious solutions from eight-band $k \cdot p$ theory, Phys. Rev. B 56 (1997) R12748–R12751.

[10] B. Fornberg, Calculation of weights in finite difference formulas, SIAM Rev. 40 (1998) 685–691.

[11] R.H. Gutierrez, P.A.A. Laura, Vibrations of non-uniform rings studied by means of the differential quadrature method, J. Sound Vib. 185 (1995) 507–513.

[12] B.N. Jiang, J. Wu, L.A. Povinelli, The origin of spurious solutions in computational electromagnetics, J. Comput. Phys. 125 (1996) 104–123.

[13] R.B. Pember, Numerical methods for hyperbolic conservation laws with stiff relaxation I. Spurious solutions, SIAM J. Appl. Math. 53 (1993) 1293–1330.

[14] J. Rappaz, J.S. Hubert, E.S. Palencia, D. Vassiliev, On spectral pollution in the finite element approximation of the elastic "membrane" shells, Numer. Math. 75 (1997) 473–500.

[15] A. Sestieri, A. Carcaterra, On the spurious solutions in complex envelope displacement analysis, J. Sound Vib. 240 (2001) 293–302.

[16] C. Shu, Differential Quadrature and its Application in Engineering, Springer-Verlag, London, 2000.

[17] C. Shu, C.M. Wang, Treatment of mixed and nonuniform boundary conditions in GDQ vibration analysis of rectangular plates, Engrg. Struct. 21 (1999) 125–134.

[18] Y. Wang, Y.B. Zhao, G.W. Wei, A note on the numerical solution of high-order differential equations, J. Comput. Appl. Math. 159 (2003) 387–398.

[19] G.W. Wei, Discrete singular convolution for solution of the Fokker–Planck equations, J. Chem. Phys. 110 (1999) 8930–8942.

[20] G.W. Wei, Y.B. Zhao, Y. Xiang, Discrete singular convolution and its application to the analysis of plates with internal supports. I Theory and algorithm, Int. J. Numer. Methods Engrg. 55 (2002) 913–946.

[21] S. Zhao, G.W. Wei, Comparison of the discrete singular convolution and three other numerical schemes for solving Fisher's equation, SIAM J. Sci. Comput. 25 (2003) 127–147.

[22] S. Zhao, G.W. Wei, high order FDTD methods via derivative matching for Maxwell's equations with material interfaces, J. Comput. Phys. 200 (2004) 60–103.

[23] S. Zhao, G.W. Wei, Tensor product derivative matching for wave propagation in inhomogeneous media, Microwave Opt. Technol. Lett. 43 (2004) 69–77.

[24] S. Zhao, G.W. Wei, A new boundary implementation method for high-order central finite difference, preprint 2007.

[25] S. Zhao, G.W. Wei, Y. Xiang, DSC analysis of free-edged beams by an iteratively matched boundary method, J. Sound Vib. 284 (2005) 487–493.

[26] Y.C. Zhou, S. Zhao, M. Feig, G.W. Wei, High order matched interface and boundary method for elliptic equations with discontinuous coefficients and singular sources, J. Comput. Phys. 213 (2006) 1–30.